Di-neutron and the three-nucleon continuum observables

H. Witała
M. Smoluchowski Institute of Physics, Jagiellonian University, PL-30059 Kraków, Poland

W. Glöckle
Institut für Theoretische Physik II, Ruhr-Universität Bochum, D-44780 Bochum, Germany

(Received 24 April 2012; published 25 June 2012)

We investigate how strongly a hypothetical $^1S_0$ bound state of two neutrons would affect observables in neutron-deuteron reactions. To that aim we extend our momentum-space scheme of solving the three-nucleon Faddeev equations and incorporate in addition to the deuteron also a $^1S_0$ di-neutron bound state. We discuss effects induced by a di-neutron on the angular distributions of the neutron-deuteron elastic scattering and deuteron breakup cross sections. A comparison to the available data for the neutron-deuteron total cross section and elastic scattering angular distributions cannot decisively exclude the possibility that two neutrons can form a $^1S_0$ bound state. However, strong modifications of the final-state-interaction peaks in the neutron-deuteron breakup reaction seem to disallow the existence of a di-neutron.

DOI: 10.1103/PhysRevC.85.064003 PACS number(s): 21.45.Bc, 25.10.+s, 25.40.Dn

I. INTRODUCTION

The investigation of neutron-deuteron (nd) elastic scattering and the deuteron breakup observables [1] revealed a number of discrepancies between data and theoretical predictions based on either modern nucleon-nucleon potentials, such as AV18 [2]; charge-dependent (CD) Bonn [3]; and Nijm1, 2, and 93 [4]; or nuclear forces derived in the framework of chiral effective field theory [5]. These potentials describe very accurately the existing nucleon-nucleon (NN) database with χ^2 values per data point close to 1. Some of these discrepancies can be explained by including in the three-nucleon (3N) Hamiltonian in addition to pairwise interactions also three-nucleon forces (3NF's). However, some observables still cannot be explained and they reveal a high insensitivity to the underlying dynamics, especially to the choice of 3NF's. The neutron-neutron (nn) quasi-free-scattering (QFS) configuration in the kinematically complete nd breakup is one such example. Another one is the symmetrical space-star (SST) geometry. The nn QFS refers to the kinematical configuration in which the outgoing proton is at rest in the laboratory system. In the case of SST the momenta of the three outgoing nucleons have equal magnitude with an angle of 120° between two adjacent momenta. In the three-nucleon center-of-mass (c.m.) system these momenta form a plane perpendicular to the incoming nucleon momentum. In the QFS and SST configurations the theoretical predictions underestimate the data by about 20%. Together with the fact that the cross section in these configurations is dominated by $^1S_0$ and $^3S_1$ contributions this led to the conjecture that something might be wrong with the $^1S_0$ nn force, and that two neutrons may even form a bound state [6,7].

These observations motivated us to investigate the consequences a possible $^1S_0$ di-neutron would have on different observables in the nd reaction, and to what degree the available nd data allow for such a bound state. Specifically, we would like to find out whether or not the existence of the di-neutron could help resolve the discrepancies referred to above in the QFS and SST nd breakup configurations.

In Sec. II we extend our formulation of the momentum-space treatment of the 3N Faddeev equations to include, in addition to the deuteron, also the $^1S_0$ bound state of two neutrons. Changing the strength of the $^1S_0$ nn interaction of the CD Bonn potential, we produce a number of forces that allow two neutrons to be bound with different di-neutron binding energies. In Sec. III we present theoretical predictions based on the solution of the 3N Faddeev equations and compare them to the available nd data. We summarize and conclude in Sec. IV.

II. FADDEEV EQUATIONS WITH DI-NEUTRON

We shortly present the basics of our momentum-space treatment of the 3N Faddeev equations and calculations of the transition operators for different reactions in the 3N continuum based on solutions of these equations. For a detailed presentation we refer to Refs. [1,8]. We put an emphasis on changes of the standard approach in the case when, beside the deuteron, also one additional bound state appears in some partial wave.

For calculating processes initiated from a state $|\Phi_{1,1}\rangle \equiv |\vec{q}_0, \phi_d\rangle$, which describes the neutron moving with relative momentum $\vec{q}_0$ with respect to the deuteron with wave function ϕ_d, one needs the state $|T\rangle$ which fulfills the 3N Faddeev equation

$$|T\rangle = tP|\Phi_{1,1}\rangle + tPG_0|T\rangle, \tag{1}$$

where P is defined in terms of the transposition operators of three nucleons, $P = P_{12}P_{23} + P_{13}P_{23}$. The quantity G_0 is the free 3N propagator and t is the two-nucleon off-shell t matrix. Knowing $|T\rangle$, the breakup as well as the elastic nd scattering amplitudes can be obtained by quadratures in the standard manner [1]. Namely, the transition amplitude for elastic scattering $\langle\Phi'_{1,1}|U|\Phi_{1,1}\rangle$ was given by the authors of Refs. [1,8]

$$\langle\Phi'_{1,1}|U|\Phi_{1,1}\rangle = \langle\Phi'_{1,1}|PG_0^{-1}|\Phi_{1,1}\rangle + \langle\Phi'_{1,1}|P|T\rangle, \tag{2}$$

and for breakup $\langle\Phi_0|U_0|\Phi_{1,1}\rangle$ by

$$\langle\Phi_0|U_0|\Phi_{1,1}\rangle = \langle\Phi_0|(1+P)|T\rangle. \tag{3}$$

The state $|\Phi_0\rangle \equiv \frac{1}{\sqrt{2}}(1-P_{23})|\vec{p}\vec{q}\rangle$ corresponds to a kinematically complete breakup configuration described by the standard Jacobi momenta $\vec{p}$ and $\vec{q}$, and $|\Phi'_{1,1}\rangle$ is the outgoing state in elastic scattering with a new direction of the relative neutron-deuteron momentum $\vec{q}'_0$, but with the same magnitude as in the initial channel $|\vec{q}'_0| = |\vec{q}_0|$.

Introducing the momentum space 3N partial-wave basis $|pq\alpha\rangle \equiv |pq(ls)j(\lambda 1/2)I(jI)J(t1/2)T\rangle$ with the two-body subsystem orbital angular momentum l, spin s, total angular momentum j, and isospin t, coupled with the corresponding quantum numbers of the spectator nucleon (the orbital angular momentum λ, spin $1/2$, total angular momentum I, and isospin $1/2$) to the total angular momentum J and isospin T of the 3N system, and projecting Eq. (1) on these states, we obtain a system of coupled integral equations in two continuous variables p and q. For details of the numerical treatment of that system, and particularly of the kernel part $\langle pq\alpha|tPG_0|T\rangle$, we refer to Ref. [1].

The two-nucleon t matrix conserves the spectator momentum q and all discrete quantum numbers except for the orbital angular momentum l

$$\begin{aligned}&\langle pq\alpha|t(E)|p'q'\alpha'\rangle \\ &= \frac{\delta(q-q')}{q^2} t_{l_\alpha l_{\tilde{\alpha}}}^{s_\alpha j_\alpha t_\alpha}\left(pp'; E(q) = E - \frac{3}{4m}q^2\right) \\ &\quad \times \delta_{s_\alpha s_{\alpha'}}\delta_{j_\alpha j_{\alpha'}}\delta_{t_\alpha t_{\alpha'}}\delta_{\lambda_\alpha\lambda_{\alpha'}}\delta_{I_\alpha I_{\alpha'}}\end{aligned} \tag{4}$$

and it has a pole in channels α for which the two-nucleon subsystem has a bound state.

In the channels $|\alpha\rangle = |\alpha_d\rangle$, which contain the two-body ${}^3S_1$–${}^3D_1$ states, we extract the deuteron pole. Thus we define

$$t_{l_\alpha l_{\tilde{\alpha}}}^{s_\alpha j_\alpha t_\alpha}[p, p'; E(q)] \equiv \frac{\hat{t}_{l_\alpha l_{\tilde{\alpha}}}^{s_\alpha j_\alpha t_\alpha}[p, p'; E(q)]}{E + i\epsilon - \frac{3}{4m}q^2 - \epsilon_d} \tag{5}$$

for the deuteron quantum numbers $s_\alpha = j_\alpha = 1, t_\alpha = 0, l_\alpha, l_{\tilde{\alpha}} = 0, 2$ and keep t as it is otherwise. Obviously that pole property carries over to the T amplitude, and we define just for the $|\alpha\rangle = |\alpha_d\rangle$ channels

$$\langle pq\alpha|T\rangle = \frac{\langle pq\alpha|\hat{T}\rangle}{E + i\epsilon - \frac{3}{4m}q^2 - \epsilon_d}. \tag{6}$$

Since the energy E of the 3N system is determined by the incoming neutron energy $E_{\text{c.m.}}$: $E = E_{\text{c.m.}} + \epsilon_d \equiv \frac{3}{4m}q_0^2 + \epsilon_d$, the deuteron pole occurs at $q = q_0$.

If besides the deuteron an additional bound state exists in some two-nucleon partial wave state, one needs to extract in channels $|\alpha\rangle$, which contain that two-nucleon state, the corresponding pole of the t matrix by performing the same procedure as for the deuteron. Let us assume that this state is a bound state of two neutrons in the ${}^1S_0$ state with wave function ϕ_{nn} and binding energy ϵ_{nn}, and let us denote by $|\Phi_{1,2}\rangle \equiv |\vec{\bar{q}}_0, \phi_{\text{nn}}\rangle$ the two-body channel built on the di-neutron, from which or to which different reactions can be initiated.

In the channels $|\alpha\rangle = |\alpha_{^1S_0}\rangle$, which contain the ${}^1S_0$ di-neutron, we define

$$\begin{aligned}t_{l_\alpha l_{\tilde{\alpha}}}^{s_\alpha j_\alpha t_\alpha}[p, p'; E(q)] &\equiv \frac{\hat{t}_{l_\alpha l_{\tilde{\alpha}}}^{s_\alpha j_\alpha t_\alpha}[p, p'; E(q)]}{E + i\epsilon - \frac{3}{4m}q^2 - \epsilon_{\text{nn}}} \\ &= \frac{\hat{t}_{l_\alpha l_{\tilde{\alpha}}}^{s_\alpha j_\alpha t_\alpha}[p, p'; E(q)]}{\frac{3}{4m}\left(\bar{q}_0^2 - q^2\right) + i\epsilon}\end{aligned} \tag{7}$$

and the di-neutron pole occurs at $q = \bar{q}_0 = \sqrt{q_0^2 + \frac{4m}{3}(\epsilon_d - \epsilon_{\text{nn}})}$. Again that pole property carries over to the T amplitude and we define for the $|\alpha\rangle = |\alpha_{^1S_0}\rangle$ channels the amplitude $\langle pq\alpha|\hat{T}\rangle$ similarly to Eq. (6). The numerical treatment of that new pole follows the treatment of the deuteron pole [1]. It requires the set of q points which, in addition to $q = q_0$ needed for the numerical treatment of the deuteron pole, contains also the $q = \bar{q}_0$ point. Since the di-neutron occurs in the neutron-neutron ${}^1S_0$ state, it implies charge independence breaking, and the resulting difference between the ${}^1S_0$ nn and np interactions requires an inclusion of the total 3N isospin component $T = 3/2$ for channels α containing ${}^1S_0$ [9] to calculate properly observables.

The existence of the ${}^1S_0$ di-neutron increases the number of possible reactions within the 3N system, and therefore, necessitates a generalization of the unitarity relation to include those additional processes. It has the form

$$\begin{aligned}&\langle\Phi_{1,a}|U|\Phi_{1,a'}\rangle^* - \langle\Phi_{1,a'}|U|\Phi_{1,a}\rangle \\ &= 2\pi i \sum_{b=1,2}\int d^3q \langle\Phi_{\vec{q},b}|U|\Phi_{1,a'}\rangle^*\delta\left(E_{\vec{q}}^b - E_{\vec{q}}\right) \\ &\quad \times \langle\Phi_{\vec{q},b}|U|\Phi_{1,a}\rangle + 2\pi i/6\int d^3p d^3q \langle\Phi_0|U_0|\Phi_{1,a'}\rangle^* \\ &\quad \times \delta(E_{pq} - E_{\vec{q}})\langle\Phi_0|U_0|\Phi_{1,a}\rangle,\end{aligned} \tag{8}$$

with $a = 1$ and 2 for the deuteron and di-neutron channels, respectively. One can choose $a' = 1$ or $a' = 2$ and $a = 1$ or $a = 2$. For $a = a' = 1$ this leads on the left side to the forward scattering amplitude and on the right to the total cross section. The energies $E_{\vec{q}}^b = E_{\vec{q}} + E_b$ are given by the binding energies of the deuteron $E_1 = \epsilon_d$ or di-neutron $E_2 = \epsilon_{\text{nn}}$.

The angular distribution for the process $n + d \to p +$ di-neutron is given by the transition amplitude $\langle\Phi_{1,2}|U|\Phi_{1,1}\rangle$

$$\begin{aligned}&\frac{d\sigma}{d\Omega}(n + d \to p + \text{di-neutron}) \\ &= \left(\frac{2m}{3}\right)^2 (2\pi)^4 \frac{\bar{q}_0}{q_0}\sum_{m_p m_n m_d} |\langle\Phi_{1,2}|U|\Phi_{1,1}\rangle|^2,\end{aligned} \tag{9}$$

where the PG_0^{-1} and PT contributions to U are given by

$$\begin{aligned}\langle\Phi_{1,2}|PG_0^{-1}|\Phi_{1,1}\rangle &= \langle\phi_{nn}, m_p, \vec{\bar{q}}_0|PG_0^{-1}\,|\phi_d, m_n, m_d, \vec{q}_0||\hat{z}\rangle \\ &= \frac{2}{\sqrt{4\pi}}\left[\epsilon_d - \frac{1}{m}\left(\frac{1}{4}q_0^2 + \bar{q}_0^2 + \vec{q}_0\cdot\vec{\bar{q}}_0\right)\right]\left(\frac{1}{2}\frac{1}{2}1\middle|-\frac{1}{2},-\frac{1}{2},-1\right)\left(\frac{1}{2}\frac{1}{2}0\middle|-\frac{1}{2},\frac{1}{2},0\right) \\ &\times \phi_{\rm nn}\left(\left|\vec{q}_0 + \frac{1}{2}\vec{\bar{q}}_0\right|\right)\sum_{l=0,2}(l11|m_d + m_n - m_p, -m_n + m_p, m_d)\left(\frac{1}{2}\frac{1}{2}1\middle|-m_n, m_p, -m_n + m_p\right) \\ &\times \left(\frac{1}{2}\frac{1}{2}0\middle|m_n, -m_n, 0\right)\phi_l^d\left(\left|\frac{1}{2}\vec{q}_0 + \vec{\bar{q}}_0\right|\right)Y_{l,m_d+m_n-m_p}\left(\frac{1}{2}\vec{q}_0 + \vec{\bar{q}}_0\right) \qquad (10)\end{aligned}$$

and

$$\begin{aligned}\langle\Phi_{1,2}|P|T\rangle &= \langle\phi_{\rm nn}, m_p, \vec{\bar{q}}_0|P|T\rangle \\ &= \sum_{J^\pi M}\sum_{\alpha'\alpha_0}\delta_{I_0 J}\delta_{l_0 0}\delta_{s_0 0}\delta_{j_0 0}\left(\lambda_0\frac{1}{2}I\middle|M-\mu',\mu',M\right)\left(1\frac{1}{2}T_0\middle|-1,\frac{1}{2},-\frac{1}{2}\right)Y_{\lambda_0,M-\mu'}(\hat{\bar{q}}_0) \\ &\times \int_0^\infty q'^2 dq' \int_{-1}^{1} dx\,\phi_{\rm nn}(\pi_1)\frac{G_{\alpha_0,\alpha'}(\bar{q}_0,q',x)}{\pi_1^{l_0}\pi_2^{l_{\alpha'}}}\left\langle\pi_2, q', \alpha'|T\right\rangle, \qquad (11)\end{aligned}$$

with

$$\begin{aligned}\pi_1 &= \sqrt{q'^2 + \frac{1}{4}\bar{q}_0^2 + q'\bar{q}_0 x}, \\ \pi_2 &= \sqrt{\bar{q}_0^2 + \frac{1}{4}q'^2 + q'\bar{q}_0 x}. \end{aligned} \qquad (12)$$

Here it was assumed that the relative neutron-deuteron momentum $\vec{q}_0$ in the incoming channel is directed along the z axis. The standard convention for isospin projections was used: $-\frac{1}{2}$ for the neutron and $+\frac{1}{2}$ for the proton. In Eq. (11) the channels α_0 contain the di-neutron two-nucleon subsystem quantum numbers with isospin $t_0 = 1$ and its projection $\nu_{t_0} = -1$ and the total isospin T_0 of the 3N system with $T_0 = \frac{1}{2}$ or $T_0 = \frac{3}{2}$. The geometrical coefficient $G_{\alpha_0,\alpha'}(\bar{q}_0, q', x)$ stems from the matrix elements of the permutation operator P [1].

III. RESULTS

In the following we present and compare to the available nd data the theoretical predictions for the cross sections in elastic nd scattering and breakup observables assuming different $^1S_0$ nn forces. We take the CD Bonn [3] potential as the NN interaction and multiply its $^1S_0$ nn component by a factor λ to generate a number of $^1S_0$ nn forces among which some provide binding of two neutrons. In Table I we show values of the nn scattering length $a_{\rm nn}$, the effective range parameter $r_{\rm eff}$, and the di-neutron binding energy $\epsilon_{\rm nn}$ for different λ values. Changing λ from 0.9 to 1.4 leads to nn $^1S_0$ forces with different, negative as well as positive, values of the scattering length. To see whether our conclusions depend on the particular $^1S_0$ nn potential used, and on the method applied to generate the nn bound state, we also performed calculations with a chiral NN potential in next-to-leading order (NLO) of the chiral expansion [5], and by adjusting its $^1S_0$ nn low-energy constants to obtain a di-neutron with a given binding energy.

A. Total cross section

The results for the nd total cross section are shown in Fig. 1, and for a number of energies, they are also presented in Table II. The theoretical predictions obtained with different nn $^1S_0$ forces are compared to numerous data taken over many years. Up to about 100 MeV there is nice agreement between all data and theory based on the CD Bonn potential, especially with the very precise data of Ref. [10]. When instead of the original CD Bonn $^1S_0$ nn force the modified interaction with factor $\lambda = 0.9$ is taken, the resulting cross-section values seem to be not excluded by the total cross-section data. However, for $\lambda = 1.21$, with the di-neutron binding energy $\epsilon_{\rm nn} = -144$ keV, the predicted total cross section for energies up to ≈ 10 MeV differs from the data by about three standard deviations. At higher energies, the calculated total cross section clearly deviates by more than three standard deviations from the data. Increasing the factor λ to 1.3 or 1.4 leads to total cross-section values that strongly overestimate the data.

In Figs. 2 and 3 we compare theoretical predictions for the total elastic scattering and breakup cross sections, respectively, with the corresponding data. For the elastic scattering component of the total cross section (see Fig. 2), the theoretical predictions with different nn $^1S_0$ forces are close to

TABLE I. The di-neutron binding energy $\epsilon_{\rm nn}$, the nn scattering length $a_{\rm nn}$, and the effective range parameter $r_{\rm eff}$ for different factors λ by which the nn $^1S_0$ component of the CD Bonn potential was multiplied.

λ	$\epsilon_{\rm nn}$ [MeV]	$a_{\rm nn}$ [fm]	$r_{\rm eff}$ [fm]
0.9	–	−8.25	3.12
1.0	–	−18.80	2.82
1.19	−0.099	+21.69	2.39
1.21	−0.144	+18.22	2.35
1.3	−0.441	+10.95	2.20
1.4	−0.939	+7.87	2.07

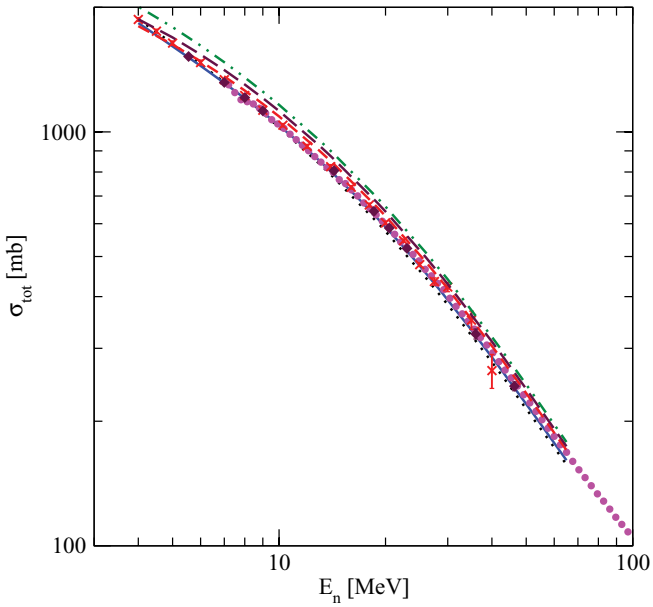

FIG. 1. (Color online) Total cross section for neutron-deuteron scattering as a function of neutron laboratory energy. Different curves show the sensitivity of the total cross section to changes of the nn $^1S_0$ force component. Those changes were induced by multiplying the $^1S_0$ nn matrix element of the CD Bonn potential by the factor λ. The solid (blue) curve is the full result based on the original CD Bonn potential (λ = 1.0) and all partial waves with 2N total angular momenta up to $j_{max} = 3$ included. The (black) dotted, (red) short-dashed, (maroon) long-dashed, and (green) double-dot-dashed curves correspond to λ = 0.9, 1.21, 1.3, and 1.4, respectively. The (magenta) circles, (red) x-es, and (maroon) diamonds are nd data of Refs. [10–12].

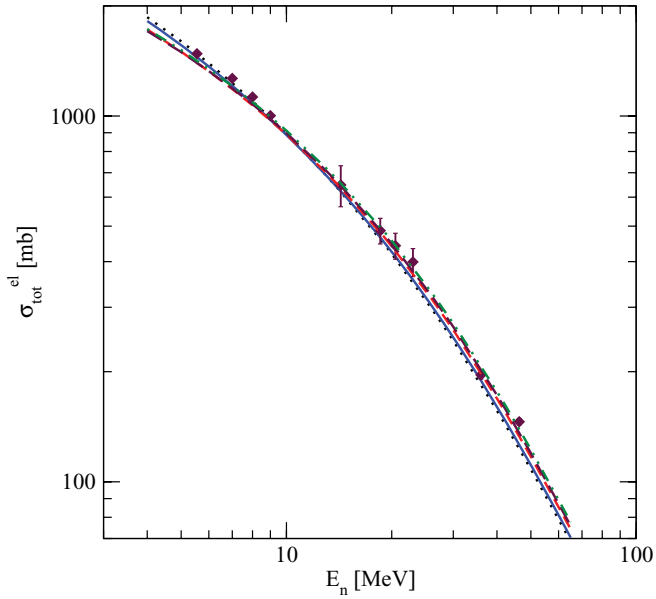

FIG. 2. (Color online) Total neutron-deuteron elastic scattering cross section as a function of neutron laboratory energy. Different curves show the sensitivity of that cross section to changes of the nn $^1S_0$ force component. For their description see Fig. 1. The (maroon) diamonds are nd data of Ref. [12].

each other and they agree with the data at energies up to about $E_n \approx 20$ MeV. However, at energies above $E_n \approx 20$ MeV the calculated cross-section values for λ > 1 start to deviate from the standard CD Bonn and λ = 0.9 values and the data seem to prefer larger values of λ.

TABLE II. The theoretical (evaluated at the nucleon laboratory energy E_{th}) and experimental (taken at E_{exp}) nd total cross section. The theoretical values were obtained with the CD Bonn potential, where the $^1S_0$ nn component was multiplied by the factor λ.

E_{th} [MeV]	σ_{exp} [mb]	E_{exp} [MeV]	$\sigma_{th}^{\lambda=0.9}$ [mb]	$\sigma_{th}^{\lambda=1.0}$ [mb]	$\sigma_{th}^{\lambda=1.21}$ [mb]	$\sigma_{th}^{\lambda=1.3}$ [mb]	$\sigma_{th}^{\lambda=1.4}$ [mb]
8.0	1207 ± 13	8.0 [13]	1203.4	1205.6	1258.5	1301.4	1353.5
	1213.3 ± 5.58	8.038 [14]					
	1224 ± 10	8.0 [11]					
10.0	1055 ± 10	10.0 [13]	1026.4	1036.1	1089.9	1123.7	1162.5
	1051.1 ± 6.9	10.026 [14]					
	1045.0 ± 3.4127	9.9218 [10]					
13.0	867 ± 12	12.995 [13]	837.96	851.76	900.91	926.56	954.72
14.1	803 ± 14	14.1 [15]	783.94	798.25	845.37	868.91	894.52
	790 ± 20	14.1 [16]					
	809 ± 6	14.1 [17]					
	778 ± 22	14.1 [18]					
	806 ± 6	14.1 [18]					
	810 ± 30	14.2 [19]					
19.0	627.96 ± 12.16	18.932 [14]	603.47	617.55	655.92	673.20	691.76
	632 ± 14	19.01 [20]					
26.0	455 ± 12	26.015 [13]	444.41	456.18	485.43	497.83	511.16
	451.47 ± 17.72	26.082 [14]					
42.5	267.7 ± 3.9	42.5 [21]	259.24	266.35	283.32	290.27	297.88
65.0	166.5 ± 2.9	63.5 [21]	157.24	160.95	170.27	173.96	178.13
	161.7 ± 2.8	66.5 [21]					
	168.27.0 ± 0.48333	65.039 [10]					

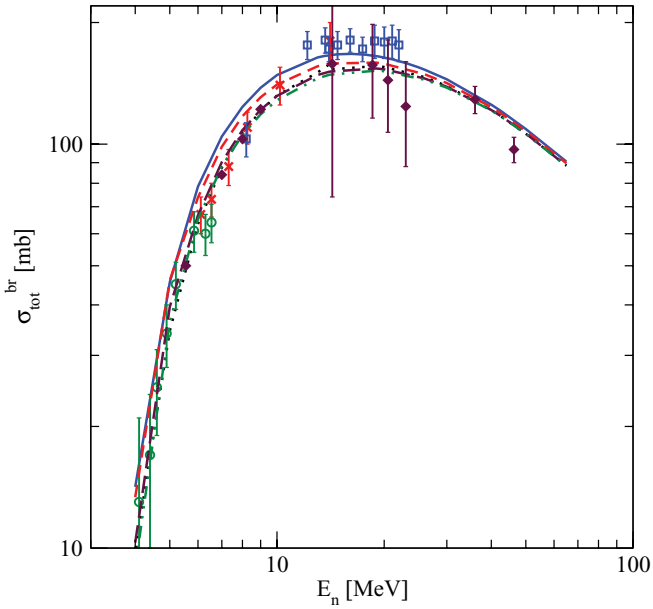

FIG. 3. (Color online) Total neutron-deuteron breakup cross section as a function of neutron laboratory energy. Different curves show the sensitivity of that cross section to changes of the nn $^1S_0$ force component. For their description see Fig. 1. The (red) crosses, (green) circles, (blue) squares, and (maroon) diamonds are nd data of Refs. [12,22–24].

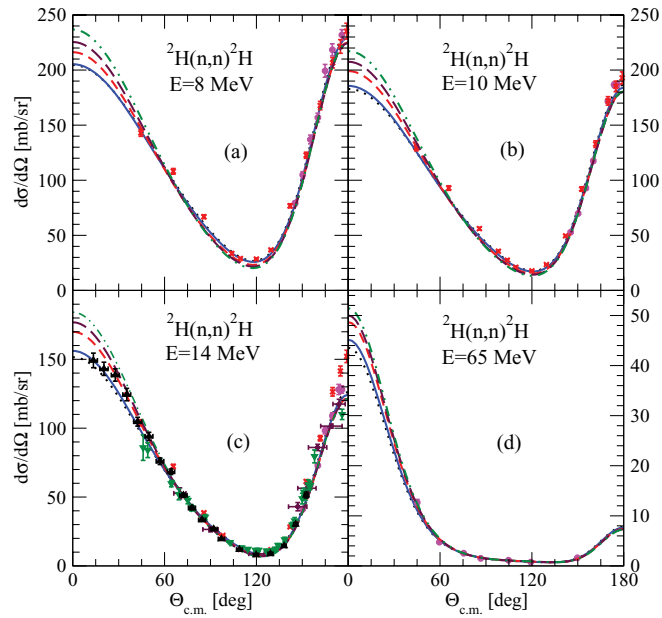

FIG. 4. (Color online) Neutron-deuteron elastic scattering angular distributions $d\sigma/d\Omega$ at a number of incoming neutron laboratory energies. Different curves show the sensitivity to changes of the nn $^1S_0$ force component. For their description see Fig. 1. At (a)–(c) $E_n = 8$, 10, and 14 MeV the (magenta) circles and (red) x-es are nd data of Refs. [11,27]. At $E_n = 14$ MeV the (maroon) stars, (green) triangle-down, and (black) triangle-up are nd data of Refs. [12,28,29]. At (d) $E_n = 65$ MeV the (blue) circles are $E_n = 66$ MeV nd data of Ref. [30].

For the total breakup cross section (see Fig. 3) the data seem to be compatible with all theoretical predictions with the exception of the data from Ref. [24]. These data taken in the energy range 12 MeV $< E_n <$ 22 MeV clearly support the CD Bonn potential prediction. However, they do not exclude definitely cross-section values obtained with $\lambda = 1.21$.

At low energies the nd interaction is parameterized by the doublet $^2a_{\rm nd}$ and quartet $^4a_{\rm nd}$ scattering lengths. While $^2a_{\rm nd}$ is strongly influenced by 3NF's, $^4a_{\rm nd}$ is practically insensitive to such interactions [25]. In Table III we show how these scattering lengths change with the modification of the $^1S_0$ nn CD Bonn potential. While the doublet scattering length drastically changes with λ, the quartet scattering length remains practically constant under such modifications of the $^1S_0$ nn force, remaining close to the experimental value of $^4a_{\rm nd} = (6.35 \pm 0.02)$ fm [26].

TABLE III. The doublet $^2a_{\rm nd}$ and quartet $^4a_{\rm nd}$ nd scattering lengths for the different factors λ by which the nn $^1S_0$ component of the CD Bonn potential was multiplied. The calculations were done with all partial waves with the 2N total angular momenta up to $j_{\rm max} = 3$ included.

λ	$^2a_{\rm nd}$ [fm]	$^4a_{\rm nd}$ [fm]
0.9	1.51485	6.34602
1.0	0.93174	6.34600
1.21	−0.43567	6.34596
1.3	−1.18887	6.34593
1.4	−2.37605	6.34589

B. Elastic neutron-deuteron scattering

The nd elastic scattering angular distributions are shown in Fig. 4. At c.m. scattering angles $\Theta_{\rm c.m.} > 45^\circ$ different theories practically overlap and agree with the data for all four energies shown. Such a behavior is not surprising because at backward angles the exchange term PG_0^{-1}, given by the deuteron wave function, dominates the elastic scattering transition amplitude. The properties of the nn $^1S_0$ interaction should play a decisive role at forward angles. Indeed, at angles below $\Theta_{\rm c.m.} < 45^\circ$ differences between theoretical predictions based on various nn $^1S_0$ forces become notice and they increase with decreasing angle. Unfortunately, only at $E_n = 14.1$ MeV forward angles are nd elastic scattering cross-section data available, with five data points falling into that region of interest. While the two data points at the smallest angles support the CD Bonn cross section, the three at larger angles prefer increased values of λ. Precise nd elastic scattering data at forward angles are required to decide whether or not a stronger nn $^1S_0$ force is allowed.

C. Breakup

Among the numerous kinematically complete nd breakup configurations, the largest discrepancies between the theory and data have been found for the nn QFS and SST geometries. For these configurations the theoretical cross section is insensitive to the underlying dynamics and remains unchanged when the different realistic NN potentials are augmented with

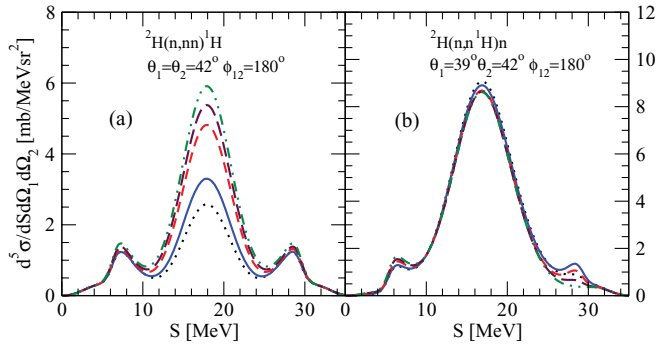

FIG. 5. (Color online) The cross section $d^5\sigma/d\Omega_1 d\Omega_2 dS$ as a function of the S-curve arc-length in the $E_n^{\rm lab} = 26$ MeV nd breakup reaction for the (a) QFS nn and (b) QFS np kinematically complete configurations of Ref. [31]. For description of curves see Fig. 1.

available 3NF's. In addition, if instead of the nn QFS the theory is compared to the only available np QFS data set [31] a nice agreement is found. The QFS and SST configurations are dominated by the $^1S_0$ and $^3S_1$ NN force components [6], which practically saturate the QFS and SST cross section at low energies [6,7]. This observation would suggest that the nn $^1S_0$ force is probably responsible for the large discrepancy between the data and theory.

For the nn and np QFS configurations we show in Fig. 5 the sensitivity to the underlying nn $^1S_0$ force. As expected, changes of that force cause drastic modifications of the nn QFS cross section, but leaving np QFS practically unaffected. As was shown in Ref. [7], such drastic modifications of the nn QFS cross section are caused by changes of the effective range parameter, which in turn are induced by the factor λ. Changes in the nn scattering length practically leave the nn QFS cross section unaffected.

In contrast to the nn QFS, the SST geometry is more stable against changes of the $^1S_0$ nn force. As shown in Fig. 6, changing the factor λ does not bring the theory closer to the data. While $\lambda = 0.9$ provides smaller SST cross-section values than the CD Bonn potential, using $\lambda > 1$ and increasing it so that the di-neutron is formed leads to cross-section values which again are below the CD Bonn potential predictions. Therefore, by modifying the $^1S_0$ nn force it is not possible to explain the large discrepancy for the SST. Because it is improbable that the deuteron properties are so badly known that the $^3S_1$–$^3D_1$ NN force component would require a modification, the source for that disagreement must be sought elsewhere. One possibility could be the indirect influence of the di-neutron on some breakup configurations by contributing in specific regions of the phase space to the breakup background.

For the $^1S_0$ nn force that allows the di-neutron to exist, the nn scattering length becomes positive. This should have a drastic influence on the nn final-state interaction (FSI) in nd breakup, where the two outgoing neutrons with equal momenta strongly interact in the $^1S_0$ state. We show in Fig. 7 the changes in the FSI peak when the nn scattering length $a_{\rm nn}$ changes from negative to positive values. For the same magnitude of $a_{\rm nn}$, the nn FSI cross section is strongly reduced for the positive sign of $a_{\rm nn}$. The question arises whether or not the existing nn FSI cross-section data can be understood if the di-neutron were to exist.

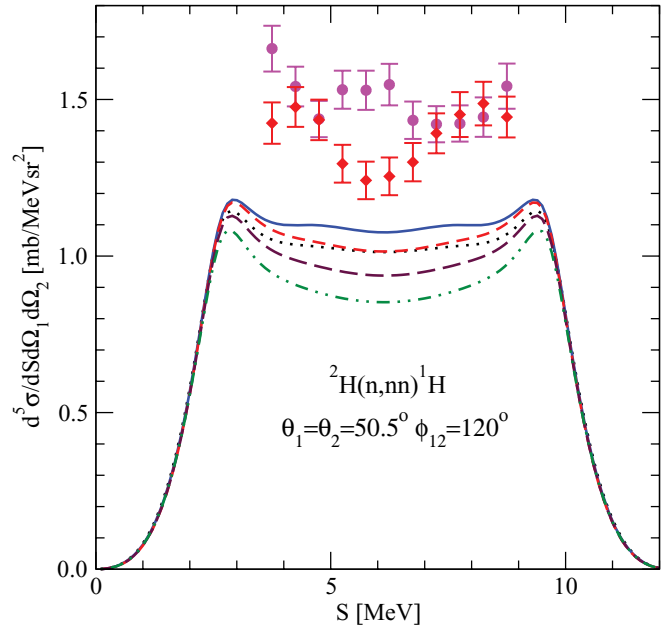

FIG. 6. (Color online) The cross section $d^5\sigma/d\Omega_1 d\Omega_2 dS$ as a function of the S-curve arc-length in the $E_n^{\rm lab} = 13$ MeV nd breakup reaction $^2H(n, {\rm nn})^1H$ for the SST configuration with the laboratory angles of the two detected neutrons $\theta_1 = \theta_2 = 52.8°$ and $\phi_{12} = 180°$. For description of curves see Fig. 1. The (magenta) solid dots and (red) x-ses are nd data of Refs. [32–34].

To answer this question, we show in Fig. 8 cross-section results for four kinematically complete nn FSI configurations for which data exist and which were analyzed by the authors of Ref. [35] with the aim of extracting the neutron-neutron scattering length. Consistent values for $a_{\rm nn}$ have been found

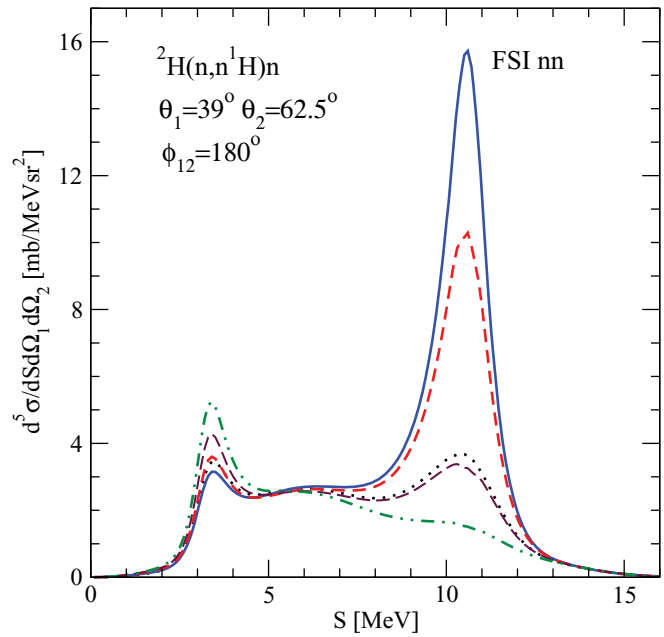

FIG. 7. (Color online) The cross section $d^5\sigma/d\Omega_1 d\Omega_2 dS$ for the $E_n^{\rm lab} = 13$ MeV nd breakup reaction $^2H(n, n^1H)n$ as a function of the S-curve length for the nn FSI configuration. For description of curves see Fig. 1.

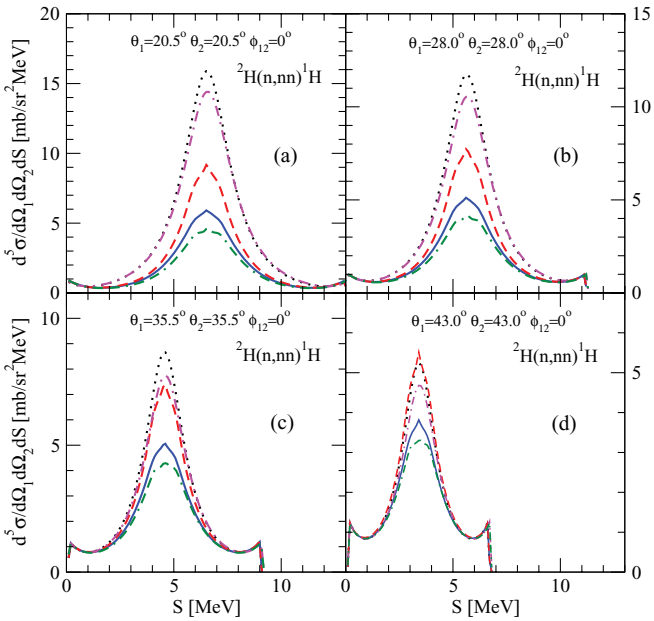

FIG. 8. (Color online) The cross section $d^5\sigma/d\Omega_1 d\Omega_2 dS$ as a function of the S-curve arc-length in the $E_n^{\rm lab} = 13$ MeV nd breakup reaction $^2H(n, {\rm nn})^1H$ for four FSI nn geometries. Different curves show the sensitivity of the cross-section values to the changes of the nn $^1S_0$ force component. Those changes were induced for the (black) dotted, (red) dashed, and (blue) solid curves by multiplying the $^1S_0$ nn matrix element of the CD Bonn potential by the factor λ. The dotted (black) curves are the full result based on the original CD Bonn potential ($\lambda = 1.0$) and all partial waves with 2N total angular momenta up to $j_{\rm max} = 3$ included. The (red) dashed and (blue) solid curves correspond to $\lambda = 1.19$ and 1.21, respectively. The (magenta) dash-dotted and (green) double-dash-dotted curves show results of Faddeev calculations performed with the chiral NLO potential and all partial waves with 2N total angular momenta up to $j_{\rm max} = 3$ included. They differ in the nn $^1S_0$ force which for the (magenta) dash-dotted curve was obtained with the constants $C_1(^1S_0) = 1.0$ and $C_2(^1S_0) = 1.0$ (original NLO potential, see text for explanation) leading to $a_{\rm nn} = -17.6$ fm and $r_{\rm eff} = 2.75$ fm. For the (green) double-dash-dotted curve we use $C_1(^1S_0) = 1.50$ and $C_2(^1S_0) = 1.29415$, resulting in $a_{\rm nn} = +17.5$ fm and $r_{\rm eff} = 2.41$ fm.

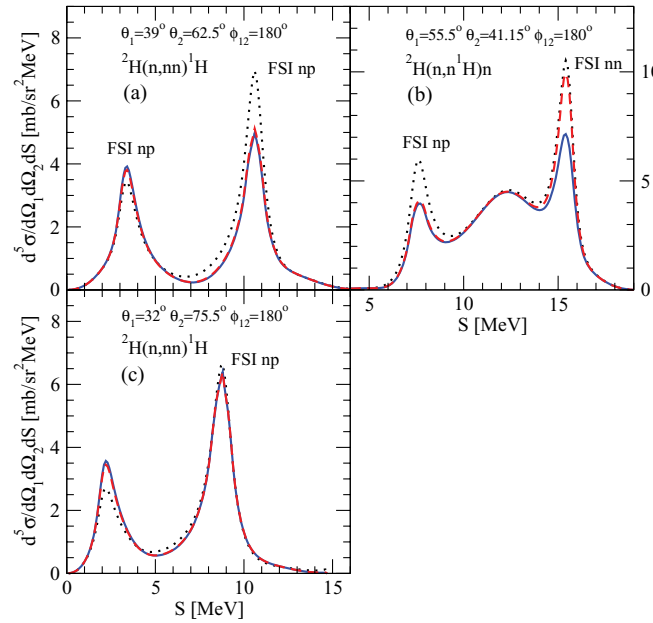

FIG. 9. (Color online) The cross section $d^5\sigma/d\Omega_1 d\Omega_2 dS$ as a function of the S-curve arc-length at $E_n^{\rm lab} = 13$ MeV for the (a), (c) $^2H(n, {\rm nn})^1H$ and (b) $^2H(n, n^1H)n$ breakup reaction and three FSI geometries. Different curves demonstrate the sensitivity of that cross section to changes of the nn $^1S_0$ force component. For their description see Fig. 8.

in each of those four configurations with the average value of $a_{\rm nn} = 18.7 \pm 0.7$ fm. As can be seen in Fig. 8, again changing $a_{\rm nn}$ to positive values, reduces significantly the nn FSI cross section. The comparison of the cross-section results obtained with $\lambda = 1.19$ and $\lambda = 1.21$ to the CD Bonn potential values clearly demonstrates that no theoretical analysis of the data of Ref. [35], using positive values of $a_{\rm nn}$, would provide consistent values for the nn scattering length in those four geometries. While the analysis of the $\theta_1 = \theta_2 = 43^\circ$ configuration would probably provide $a_{\rm nn} = +21.69$ fm, a similar analysis of the configurations at smaller $\theta_1 = \theta_2$ would provide clearly larger positive values for the nn scattering length.

In Fig. 9 we show three additional FSI configurations for which data are available. For the $^2H(n, {\rm nn})^1H$ kinematically complete breakup, the data of the authors of Ref. [33] support the CD Bonn potential cross-section predictions. Each of the two configurations given in Fig. 9 contains two np FSI peaks. The theoretical analysis of these np FSI peaks, if performed with positive values of $a_{\rm nn}$, would provide different values for the neutron-proton scattering length $a_{\rm np}$, which, in addition, would be inconsistent with the well-known experimental value for $a_{\rm np}$.

In Fig. 9 we also show the $^2H(n, n^1H)n$ breakup configuration for which data have been taken and analyzed in Ref. [36]. This geometry contains both np and nn FSI peaks. Again, the analysis of the np FSI peak, if performed with positive $a_{\rm nn}$, would provide too large magnitudes for $a_{\rm np}$.

To see how our conclusions depend on the NN potential used and on the method applied to modify the $^1S_0$ nn force, we present in Fig. 8 also cross-section values obtained with the NLO chiral perturbation theory potential of the authors of Ref. [5], including all np and nn forces up to the total angular momentum $j_{\rm max} = 3$ in the two-nucleon subsystem. The $^1S_0$ component of that interaction is composed of the one- and two-pion exchange terms and contact interactions parameterized by two parameters $\tilde{C}_{^1S_0}$ and $C_{^1S_0}$

$$V(^1S_0) = \tilde{C}_{^1S_0} + C_{^1S_0}(p^2 + p'^2). \qquad (13)$$

The standard values are $\tilde{C}_{^1S_0} = -0.1557374 \times 10^4$ GeV^2 and $C_{^1S_0} = 1.5075220 \times 10^4$ GeV^4 for the cutoff combinations $\{\Lambda, \tilde{\Lambda}\} = \{450$ MeV, 500 MeV$\}$ [5]. Changes of the nn $^1S_0$ interaction can be induced by multiplying $\tilde{C}_{^1S_0}$ with a factor $C_2(^1S_0)$ and $C_{^1S_0}$ with a factor $C_1(^1S_0)$. In Fig. 8 we present two predictions based on the NLO potential with negative [$a_{\rm nn} = -17.6$ fm—the (magenta) dash-dotted curve] and positive [$a_{nn} = +17.5$ fm—the (green) double-dash-dotted curve] values of the neutron-neutron scattering length. By

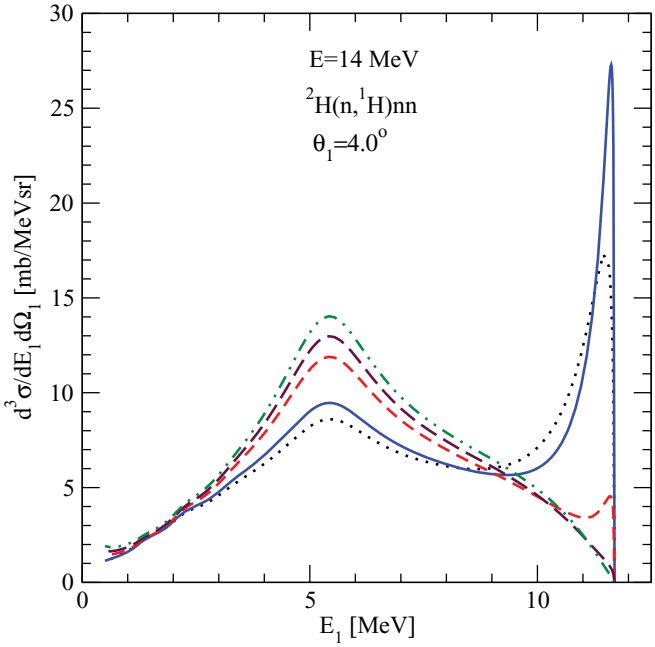

FIG. 10. (Color online) The cross section $d^3\sigma/d\Omega_1 dE_p$ at $E_n^{\rm lab} =$ 14 MeV for the kinematically incomplete $^2H(n,^1H)$nn breakup reaction as a function of the outgoing proton laboratory energy at the proton laboratory angle $\theta_1 = 4^\circ$. For a description of curves see Fig. 1.

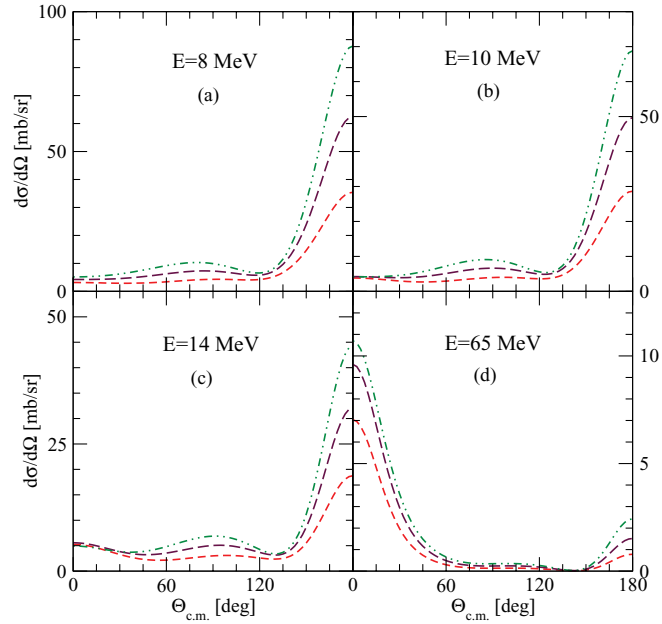

FIG. 11. (Color online) The angular distributions $d\sigma/d\Omega$ for the $^2H(n,^1H)$ di-neutron reaction at a number of incoming neutron laboratory energies. The (red) short-dashed, (maroon) long-dashed, and (green) dashed-double-dotted curves correspond to the factor $\lambda = 1.21$, 1.3, and 1.4, respectively.

comparing them with different CD Bonn potential predictions and taking into account the differences between their $a_{\rm nn}$ values, it becomes clear that both the potentials and methods used for changing the $^1S_0$ nn interaction lead to the same conclusions.

The FSI region can also be investigated in kinematically incomplete breakup measurement, in which the energy spectrum of the outgoing protons is measured at a given laboratory angle. In Fig. 10 we show modifications of the proton spectrum for 14 MeV nd breakup at a proton laboratory angle of $\theta = 4^\circ$. Here, changing the sign of $a_{\rm nn}$ leads to the disappearance of the FSI peak. In addition, at lower proton energies, the modification of $^1S_0$ nn force by factors $\lambda > 1$ significantly increases the breakup cross section.

The analysis of existing kinematically incomplete nd breakup spectra performed by the authors of Refs. [37,38] pointed to inconsistencies in the experimental data and revealed unexplained differences of more than 25% in regions of the proton energy spectrum where large numbers of different three-nucleon configurations contribute to the cross section. The question arises whether the existence of the di-neutron and the corresponding modification of the $^1S_0$ nn force can account for this observation and whether the strong FSI enhancement seen in the experimental proton spectrum provides evidence for the existence of the di-neutron. To answer this question, a theoretical Monte Carlo analysis of the experimental spectra obtained at different proton production angles, which would provide the angular distribution for the di-neutron cross section, is required. The resulting angular distribution should then be compared to the theoretical angular distribution for the $n + {}^2H \rightarrow {}^1H +$ di-neutron transition. However, in view of the results presented above for the kinematically complete nn FSI configurations, it seems highly unlikely that the analysis of kinematically incomplete spectra would provide a clear signal for the existence of the di-neutron.

D. Transition from the neutron-deuteron to the proton–di-neutron channel

For values of $\lambda = 1.21$, 1.3, and 1.4, which allow for the bound $^1S_0$ state of two neutrons, the transition to the proton–di-neutron channel is possible. In Fig. 11 we show angular distributions for the $n + d \rightarrow p +$ di-neutron reaction. The cross section for this reaction is an order of magnitude smaller than that for nd elastic scattering, with the largest cross section at backward c.m. angles for low incoming neutron energies.

In view of the discrepancies found in the nd breakup reaction, especially in the SST configuration, it would be interesting to study in which phase-space region the hypothetical di-neutron state could mostly affect the breakup configurations by contributing in an uncontrolled manner to the background. To answer this question, again Monte Carlo simulations of the specific experimental conditions are required.

IV. SUMMARY AND CONCLUSION

We investigate to what extent available nd data allow for a hypothetical $^1S_0$ bound state of two neutrons and if such a di-neutron can help explain the discrepancies between the theory and data found in some kinematically complete nd breakup configurations. To this aim we extend our numerical momentum-space treatment of the 3N Faddeev equation to

include, in addition to the deuteron also the $^1S_0$ bound state, the di-neutron. Solutions of this equation with modified nn $^1S_0$ CD Bonn forces provide predictions for the cross section in different nd reactions.

We find that the available nd data for the nd scattering total cross section are incompatible with the existence of a di-neutron with binding energy $|\epsilon_{nn}| > 100$ keV. The data for the total elastic scattering and breakup cross sections do not exclude such a possibility. Also, data for the nd elastic scattering angular distribution cannot decisively exclude such a state. However, in this case, precise data at forward angles, if available, could provide more constraints on the existence of the di-neutron.

The modifications of the $^1S_0$ nn force component cannot provide an explanation for the large discrepancy between the theory and data for the SST geometry in the nd breakup reaction. Allowing for the di-neutron provides even smaller SST cross-section values, thus increasing that discrepancy.

The transition from negative to positive nn scattering lengths leads to significant modifications of the FSI cross section. In the outgoing proton spectrum of the kinematically incomplete nd breakup positive scattering lengths cause a strong suppressing of the FSI peak at maximal proton energies. Careful Monte Carlo theoretical analyses of existing proton energy spectra are required to find out whether or not those spectra provide a clear signal for the existence of the di-neutron. However, kinematically complete FSI configurations for which data exist disallow positive values for a_{nn}.

ACKNOWLEDGMENTS

This work was supported by the Polish National Science Center under Grant No. DEC-2011/01/B/ST2/00578. It was also partially supported by the European Community-Research Infrastructure Integrating Activity "Exciting Physics Of Strong Interactions" (acronym WP4 EPOS) under the Seventh Framework Programme of EU. The numerical calculations were performed on the supercomputer cluster of the JSC, Jülich, Germany.

[1] W. Glöckle, H. Witała, D. Hüber, H. Kamada, and J. Golak, Phys. Rep. **274**, 107 (1996).
[2] R. B. Wiringa, V. G. J. Stoks, and R. Schiavilla, Phys. Rev. C **51**, 38 (1995).
[3] R. Machleidt, F. Sammarruca, and Y. Song, Phys. Rev. C **53**, 1483R (1996).
[4] V. G. J. Stoks, R. A. M. Klomp, C. P. F. Terheggen, and J. J. deSwart, Phys. Rev. C **49**, 2950 (1994).
[5] E. Epelbaum, Prog. Part. Nucl. Phys. **57**, 654 (2006).
[6] H. Witała and W. Glöckle, J. Phys. G: Nucl. Part. Phys. **37**, 064003 (2010).
[7] H. Witała and W. Glöckle, Phys. Rev. C **83**, 034004 (2011).
[8] W. Glöckle, *The Quantum Mechanical Few-Body Problem* (Springer-Verlag, Berlin, 1983).
[9] H. Witała, W. Glöckle, and H. Kamada, Phys. Rev. C **43**, 1619 (1991).
[10] W. P. Abfalterer *et al.*, Phys. Rev. Lett. **81**, 57 (1998).
[11] P. Schwarz *et al.*, Nucl. Phys. A **398**, 1 (1983).
[12] J. D. Seagrave, Phys. Rev. **97**, 757 (1955).
[13] J. C. Davis and H. H. Barschall, Phys. Rev. C **3**, 1798 (1971).
[14] J. M. Clement, P. Stoler, C. A. Goulding, and R. W. Fairchild, Nucl. Phys. A **183**, 51 (1972).
[15] H. L. Poss, E. O. Salant, G. A. Snow, and L. C. L. Yuan, Phys. Rev. **87**, 11 (1952).
[16] C. F. Cook and T. W. Bonner, Phys. Rev. **94**, 651 (1954).
[17] N. Koori, J. Phys. Soc. Jpn., **32**, 306 (1972).
[18] S. Shirato and N. Koori, Nucl. Phys. A **120**, 387 (1968).
[19] D. I. Meyer and W. Nyer, Report No. LA-1279, 5107.
[20] J. D. Seagrave and R. L. Henkel, Phys. Rev. **98**, 666 (1955).
[21] R. A. J. Riddle, A. Langsford, P. H. Bowen, and G. C. Cox, Nucl. Phys. **61**, 457 (1965).
[22] H. C. Catron *et al.*, Phys. Rev. **123**, 218 (1961).
[23] M. Holmberg, Nucl. Phys. A **129**, 327 (1969).
[24] G. Pauletta and F. D. Brooks, Nucl. Phys. A **255**, 267 (1975).
[25] H. Witała, A. Nogga, H. Kamada, W. Glöckle, J. Golak, and R. Skibiński, Phys. Rev. C **68**, 034002 (2003).
[26] W. Dilg, L. Koester, and W. Nistler, Phys. Lett. B **36**, 208 (1971).
[27] C. R. Howell *et al.*, Few-Body Syst. **16**, 127 (1994).
[28] J. C. Allred, A. H. Armstrong, and L. Rosen, Phys. Rev. **91**, 90 (1953).
[29] A. C. Berick, R. A. J. Riddle, and C. M. York, Phys. Rev. **174**, 1105 (1968).
[30] H. Rühl *et al.*, Nucl. Phys. A **524**, 377 (1991).
[31] A. Siepe *et al.*, Phys. Rev. C **65**, 034010 (2002).
[32] H. R. Setze *et al.*, Phys. Lett. B **388**, 229 (1996).
[33] H. R. Setze *et al.*, Phys. Rev. C **71**, 034006 (2005).
[34] J. Strate *et al.*, Nucl. Phys. A **501**, 51 (1989).
[35] D. E. Gonzalez Trotter *et al.*, Phys. Rev. C **73**, 034001 (2006).
[36] V. Huhn, L. Wätzold, C. Weber, A. Siepe, W. vonWitsch, H. Witała, and W. Glöckle, Phys. Rev. C **63**, 014003 (2000).
[37] W. Tornow, H. Witała, and R. T. Braun, Few-Body Syst. **21**, 97 (1996).
[38] W. Tornow, R. T. Braun, H. Witała, and N. Koori, Phys. Rev. C **54**, 42 (1996).